#### LETTER TO THE EDITOR

# Inside the Final Black Hole: Puncture and Trapped Surface Dynamics

## Christopher Evans, Deborah Ferguson, Bhavesh Khamesra, Pablo Laguna, Deirdre Shoemaker

Center for Relativistic Astrophysics and School of Physics, Georgia Institute of Technology, Atlanta, GA 30332, USA

E-mail: cevans216@gatech.edu

28 April 2020

**Abstract.** A popular approach in numerical simulations of black hole binaries is to model black holes as punctures in the fabric of spacetime. The location and the properties of the black hole punctures are tracked with apparent horizons, namely outermost marginally outer trapped surfaces (MOTSs). As the holes approach each other, a common apparent horizon suddenly appears, engulfing the two black holes and signaling the merger. The evolution of common apparent horizons and their connection with gravitational wave emission have been studied in detail with the framework of dynamical horizons. We present a study of the dynamics of the MOTSs and their punctures in the interior of the final black hole. The study focuses on head-on mergers for various initial separations and mass ratios. We find that MOTSs intersect for most of the parameter space. We show that for those situations in which they do not, it is because of the singularity avoidance property of the moving puncture gauge condition used in the study. Although we are unable to carry out evolutions that last long enough to show the ultimate fate of the punctures, our results suggest that MOTSs always intersect and that at late times their overlap is only partial. As a consequence, the punctures inside the MOTSs, although close enough to each other to act effectively as a single puncture, do not merge.

## 1. Introduction

An essential element in numerical relativity simulations involving black holes (BHs) is tracking the location and properties of the holes. A natural structure to accomplish this would be the event horizon of the BH. The problem with these horizons is that they are teleological in nature; that is, we require knowledge of the entire space-time in order to identify their location and dynamics. The alternative is to track apparent horizons (AHs) [1] since to find them one only needs the intrinsic metric and extrinsic curvature of the spacetime hypersurface at a given time. AHs can be used to determine the mass and angular momentum of the BHs [2]. Once the common AH forms during the merger, one can also estimate mass and spin multipole moments [3, 4] to quantify the rate at

which the final BH approaches equilibrium and potentially identify when the ringdown phase begins [5]. In addition, studies [6, 7, 8, 5, 9] have shown that fields at the AH are correlated with fields in the wave-zone and thus the gravitational wave (GW) signal itself.

The fate of the common AH resulting from a BH merger has been studied extensively and is fairly well understood [10, 11, 4, 5]. Generally, after a common MOTS forms it bifurcates into two surfaces. The outermost of these two surfaces expands and forms the AH for the final BH, while the innermost surface contracts. Furthermore, the two MOTSs that were initially the AHs of the two original BHs continue to exist well after the formation of the common horizon. While these three interior MOTSs have been studied in some detail [11, 12, 13, 5, 14], their ultimate fate remains uncertain and is the main focus of our work.

In this paper, we present a study to investigate the dynamics of MOTSs in the head-on collision of BHs for various separations and mass ratios, with the holes modeled as punctures [15]. We find that the MOTSs of the merging punctures will in general intersect. For the situations in which they do not intersect, we show that it is due to the singularity avoidance properties of the moving puncture gauge condition [16, 17] used in the study. Our simulations are not long enough to show the ultimate fate of the MOTSs and their punctures. At the same time, the results provide evidence that the punctures, although close enough to each other to act effectively as a single puncture, do not merge and the MOTSs do not fully overlap. Section 2 provides a review of the MOTS involved in the evolutions. In Section 3, we outline the computational methods used for the simulations. Results are given in Section 4, and Section 5 provides the conclusions.

### 2. Marginally Trapped Surfaces of Two Black Holes

We consider a spacetime foliation of spacelike hypersurfaces  $\Sigma_t$  labeled by a time parameter t. The initial slice  $\Sigma_0$  consists of two BHs at a coordinate separation d. Depending on d,  $\Sigma_t$  could have up to four MOTSs [11, 12, 13, 5, 14]. A MOTS is a closed spacelike 2-surface in which the divergence of its outgoing null normals vanishes. An AH is the outer-most of the MOTSs. For large enough d,  $\Sigma_t$  will have two nonconnected MOTSs,  $S_1$  and  $S_2$ , which correspond also to the AH of each individual BH. At a separation  $d_c$ , a slice  $\Sigma_t$  will also have a MOTS  $S_c$  surrounding  $S_1$  and  $S_2$ . Since  $S_c$  is now the outer-most MOTS, the surface is an AH, called the common AH. In time,  $S_c$  will become the event horizon of the final BH. For separations  $d < d_c$ , a MOTS  $S_i$  peels off from the interior of  $S_c$ , shrinking and hugging  $S_1$  and  $S_2$ . These four MOTSs,  $S_1$ ,  $S_2$ ,  $S_c$ , and  $S_i$ , are slices of four different dynamical horizons [10, 3, 18, 4]. However, in the case of  $S_i$ , this only applies for a short time before the surface becomes timelike [11]. For small initial separations,  $S_1$  and  $S_2$  are at all times nearly null surfaces [11], and thus to good approximation they are isolated horizons [19].

A difficulty in studying the eventual fate of  $S_1$  and  $S_2$  is that, for the coordinate

conditions typically used with punctures, the surfaces shrink after the formation of  $S_c$ , requiring progressively finer spatial resolution to properly resolve them. As a result, it is challenging to make any definitive statements as to whether or not the MOTSs exist based solely on the fact that they could not be located.

Many investigations into  $S_1$  and  $S_2$  have focused on locating them on a series of initial data slices varying their separations, avoiding the computational cost of performing high resolution simulations. Jaramillo, Ansorg, and Vasset [12] studied Bowen-York [20] initial data and found that at decreasing separations  $S_1$  and  $S_2$  merely shrink and show no indications of intersecting. Instead,  $S_i$  becomes highly distorted, and  $S_1$  and  $S_2$  'accumulate' against it. Pook-Kolb et al. [14, 21, 22] studied an analogous series of time symmetric Brill-Lindquist initial data [23, 24] and found that  $S_1$  and  $S_2$  intersect and merge with  $S_i$  at the exact moment of intersection. Schnetter, Krishnan, and Beyer [11] carried out simulations of head-on collision of Brill-Lindquist initial data. While they did lose the ability to track  $S_i$  rather early due to its high distortion, they made no statements about its ultimate fate or what happens to  $S_1$  and  $S_2$ . They did however speculate that if these three surfaces do in fact merge, it is more likely that  $S_1$  and  $S_2$  merge first to form a new surface that then merges with  $S_i$ .

#### 3. Numerical Methods

All simulations were done with our MAYA code [25, 26, 27, 28, 29, 30], which is based on the BSSN formulation of the Einstein equations [31, 16], with the moving punctures gauge condition [16, 17] and the CARPET [32, 33] adaptive mesh refinement driver. The MAYA code is our local version of the EINSTEINTOOLKIT code [34]. We use Brill-Lindquist initial data [23, 24] representing two initially at rest, non-spinning BHs with total mass  $M = m_1 + m_2$ , mass ratio  $q = m_1/m_2$ , and separated by a coordinate distance  $d_0$ . During the evolution, we use AHFINDERDIRECT [35] to locate the MOTSs.

As  $S_1$  and  $S_2$  approach each other, they will shrink in coordinate radius. The spatial resolution required to properly resolve and track them will thus increase accordingly. To ensure proper resolution, we activate additional refinement levels (one level each time the MOTS radius reduces by half) to maintain roughly the same number of points within each MOTS. When  $S_c$  is first located,  $S_1$  and  $S_2$  are each completely covered by three refinement levels, with each refinement having  $60^3$  points. The resolutions for each refinement are: M/100, M/200 and M/400. Towards the end of a simulation, we activate up to five additional refinement levels, with a resolution of M/12800 at the finest level.

Our code solves the  $\chi$  formulation of the BSSN equations [16] and enforces a floor value  $\chi \geq \chi_{\epsilon}$  to hande regions where the conformal factor diverges, e.g. at the punctures or singularities, where  $\chi = 0$ . We carried out a series of q = 1 and fixed  $d_0$  simulations in the range  $10^{-3} > \chi_{\epsilon} > 10^{-6}$ . We found that the final time  $t_f$  at which we cease locating  $S_1$  and  $S_2$  varied as  $t_f \sim \chi_{\epsilon}^{-0.05}$ . With a floor value of  $\chi_{\epsilon} = 10^{-6}$ , we obtain stable evolutions lasting  $t_f \approx 20 \, M$ .

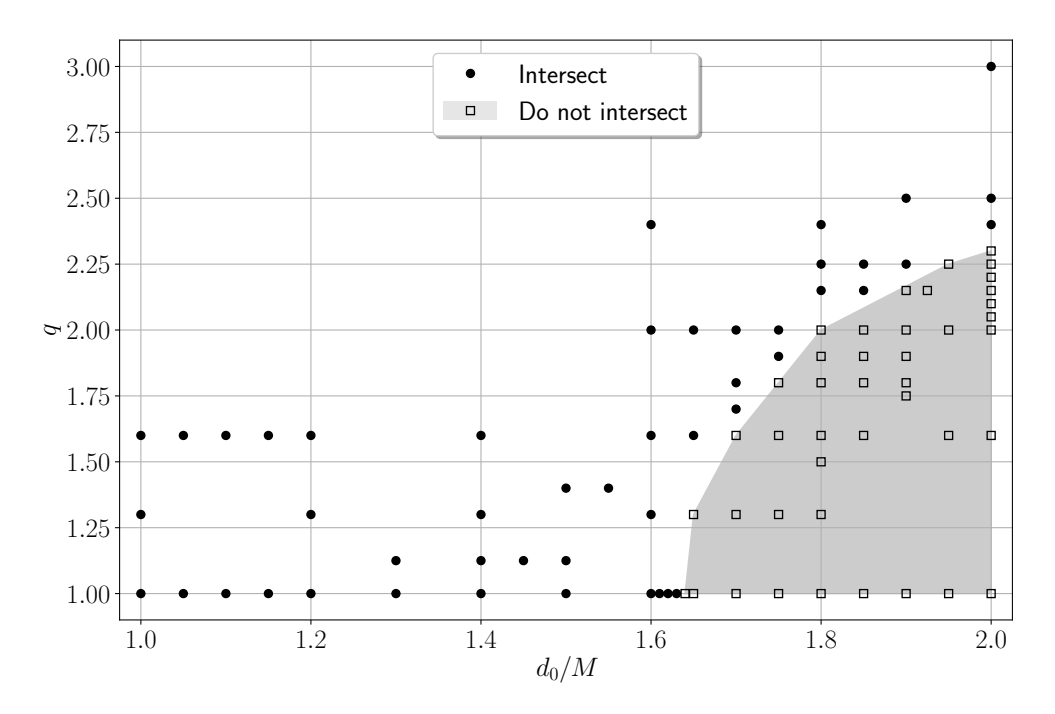


**Figure 1.** Parameter space of simulations. Simulations are characterized by mass ratio q and initial coordinate separation  $d_0$ . Cases for which  $S_1$  and  $S_2$  intersect are denoted by filled circles and non-intersecting by open boxes. In gray is the region of non-intersecting simulations.

#### 4. Results

Figure 1 shows the parameter space q vs.  $d_0$  of the simulations. There are two distinct regions: one in the lower right corner (shaded gray) in which  $S_1$  and  $S_2$  do not intersect and the rest in which they do. The boundary separating these two regions is  $q \approx 1.135 + \sqrt{4.065 (d_0/M) - 6.674}$ .

Since all the simulations are head-on collisions with the holes along the z-axis, we track the coordinate separation between  $S_1$  and  $S_2$  with  $\Delta z = z_1 - z_2$  where  $z_1$  and  $z_2$  are respectively the z-components at the surface of  $S_1$  and  $S_2$  that face each other. The coordinate origin is set at the center of mass of the initial configuration. Initially,  $z_1 > 0$  and  $z_2 < 0$ . Thus, when the two surfaces intersect,  $z_1 < z_2$ , and  $\Delta z$  becomes negative. Figure 2 shows for a few q = 1 cases  $|\Delta z|$  as a function of coordinate time t. The left panel shows three cases in which  $S_1$  and  $S_2$  intersect. The time axis has been shifted so the cases align when the surfaces intersect at time  $t_*$ , which depends on  $d_0$ . The right panel shows three other cases in which  $S_1$  and  $S_2$  do not intersect. The panels show that at late times the separation for the non-intersecting cases and the overlap for the intersecting cases both decrease as  $|\Delta z| \sim e^{-t/\lambda}$ . The same exponential decay extends to the  $q \neq 1$  cases. For all cases, we find that  $\lambda \approx 2M$ . The exponential decay in the surface separation is also present in the coordinate separation, d, of the two punctures. Shortly after the formation of  $S_c$ , we find again that  $d \propto e^{-t/\lambda}$  with  $\lambda \approx 2M$ .

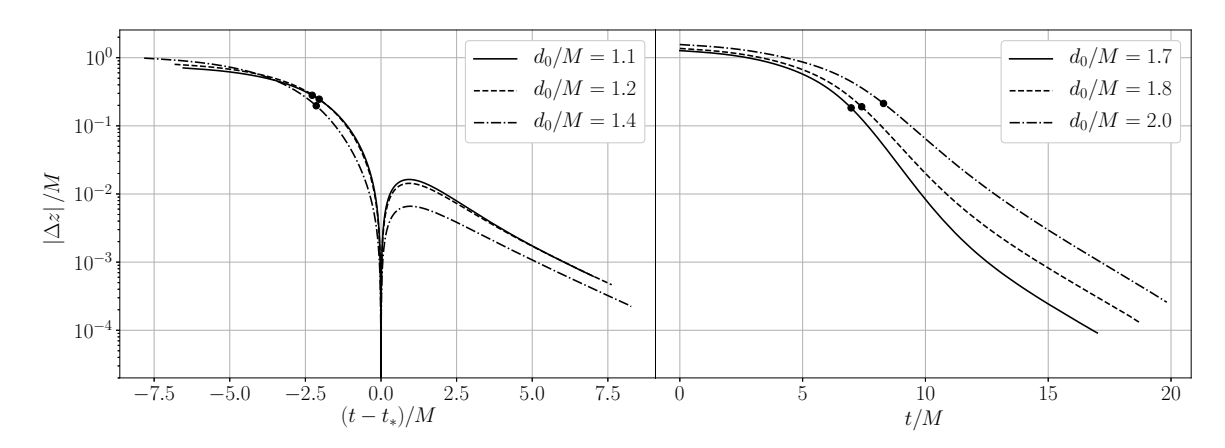


Figure 2. Coordinate separation  $|\Delta z|$  between  $S_1$  and  $S_2$  for a few q = 1 examples as a function of coordinate time t. The left panel depicts three intersecting cases aligned at the time of intersection. The right panel shows three non-intersecting cases. Solid dots denote the time at which the common AH appears.

To understand the exponential decay in the separation between  $S_1$  and  $S_2$  as well as between the punctures, we recall that in the moving puncture gauge the lapse function  $\alpha$  satisfies the 1 + log type slicing condition:  $(\partial_t - \beta^i \partial_i) \alpha = -n\alpha K$ , with  $\beta^i$  the shift vector, K the trace of the extrinsic curvature, and n a constant. As is customary, we choose n=2. With this choice, stationary slices of a single Schwarzschild puncture are given by a family of trumpet slices [36], for which the surface of zero isotropic radius (the trumpet surface) has a non-zero areal radius, and the lapse on the trumpet surface vanishes, thus avoiding the singularity at the puncture. With the moving puncture gauge, the position of the punctures  $x_{1,2}^i$  are found from integrating  $\partial_t x_{1,2}^i = -\beta_{1,2}^i$  [16]. Since for the Schwarzschild trumpet slices,  $\beta^r = r/\lambda$  near the puncture [36, 37], the radial coordinate distance to each puncture is given by  $r_{1,2} \propto e^{-t/\lambda}$ , with the decay rate  $\lambda$  computed from  $\lambda^2 = \frac{1}{r} \beta^r \partial_r \beta^r$ . Substituting the solution for  $1 + \log$  trumpet slices found by Hannam et al. [38] into this expression yields  $(\lambda/M)^2 \approx (R_0/M)^3/(2-R_0/M)$ , in which  $R_0 \approx 1.3124 \, M$ . This gives  $\lambda \approx 1.82 \, M$ , which is consistent with our numerical value from our simulations. The minor disagreement is easily explained by the fact that our numerical simulations do not reach full stationarity before completion and the shift vector is evaluated slightly away from the puncture.

To demonstrate how the lapse function is connected to the behavior observed in  $S_1$  and  $S_2$ , we show in Figure 3 the lapse function at the origin,  $\alpha_0$ , as a function of coordinate time t (left panel) and as function of  $\Delta z$  (right panel). Two cases are plotted: one in which the surfaces do not intersect  $(d_0/M=2)$  and another in which they do  $(d_0/M=1)$ . It is clear from the left panel that in both cases the lapse eventually collapses and thus halts the evolution. The difference on how the collapse proceeds in each case and affects the final outcome is more evident in the right panel. We see in this panel that at  $\Delta z \approx 0.42$  both cases are at the same separation. The solid dots in the left panel label  $\alpha_0$  at this separation. For the non-intersecting  $(d_0/M=2)$  case,

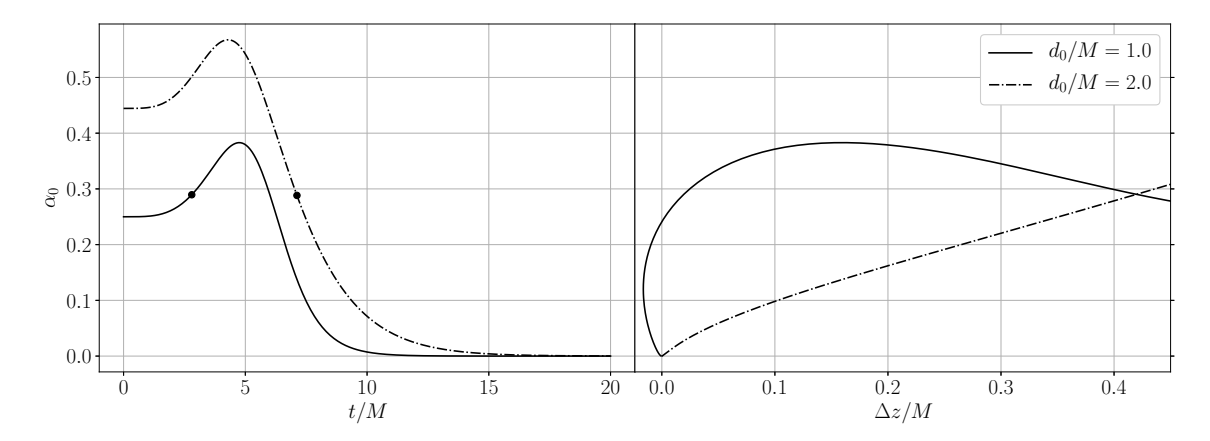
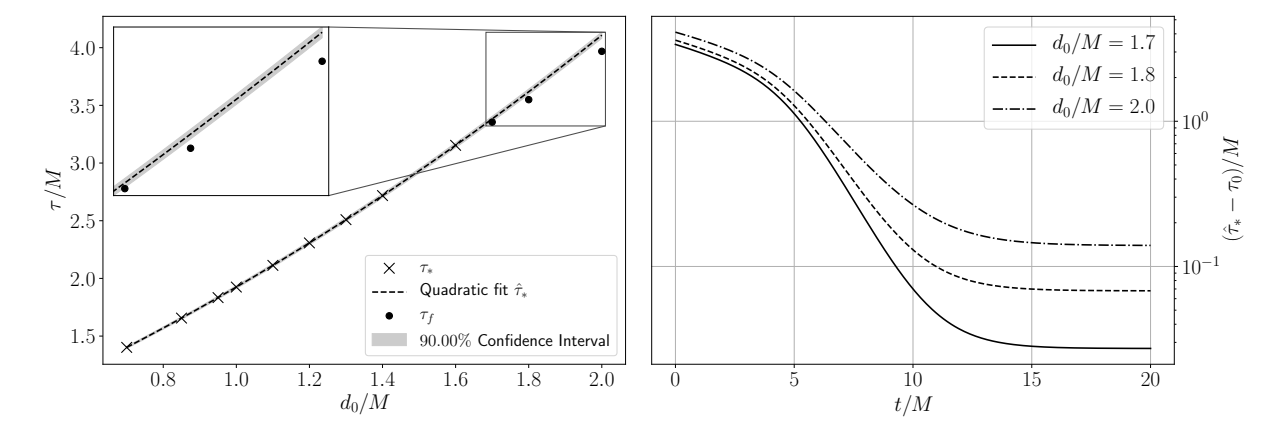


Figure 3. Lapse at the coordinate origin  $\alpha_0$  for q=1 and  $d_0/M=1$ , 2. The left panel shows how  $\alpha_0$  changes as a function of coordinate time t. The right panel shows how  $\alpha_0$  changes with  $\Delta z$ . For  $d_0/M=2$ , by the time  $\Delta z=0$ , the lapse has already collapsed. In contrast, for  $d_0/M=1$ ,  $\Delta z=0$  is reached when  $\alpha_0\approx 0.25$ . After this point, as  $\alpha_0$  collapses,  $\Delta z$  reaches a minimum and at late times  $\Delta z\to 0$ .



**Figure 4.** Left panel shows proper time  $\tau_*$  (crosses) at the origin when  $\mathcal{S}_1$  and  $\mathcal{S}_2$  intersect at time  $t_*$  for q=1 as a function of  $d_0$ . Included is also a quadratic fit  $\hat{\tau}_*$  and in gray the 90% confidence interval. With solid dots are the proper time  $\tau_f$  elapsed at the origin by the end of the simulations for three non-intersecting cases. The right panel shows  $\hat{\tau}_* - \tau_0$  as a function of t for those three non-intersecting cases.

 $\alpha_0$  is already starting to collapse. On the other hand, for the intersecting  $(d_0/M = 1)$  case,  $\alpha_0$  is still growing; thus, the evolution lives longer and the surfaces are able to intersect before the end of the simulation. What is also interesting is that the degree of intersection or surface overlap reaches a maximum and then decreases as the lapse enters collapse. As we will show later, this is a coordinate effect.

To further support the view about the effect of the lapse, we have measured the proper time  $\tau_0(t) = \int_{t=0}^t \alpha_0 dt'$  at the origin. The left panel in Fig. 4 shows with crosses  $\tau_* \equiv \tau_0(t_*)$ , where  $t_*$  is the time when  $\mathcal{S}_1$  and  $\mathcal{S}_2$  intersect. Also plotted is a quadratic fit  $\hat{\tau}_*/M = 0.337 (d_0/M)^2 + 1.170 (d_0/M) + 0.417$  and in gray the 90% confidence interval.

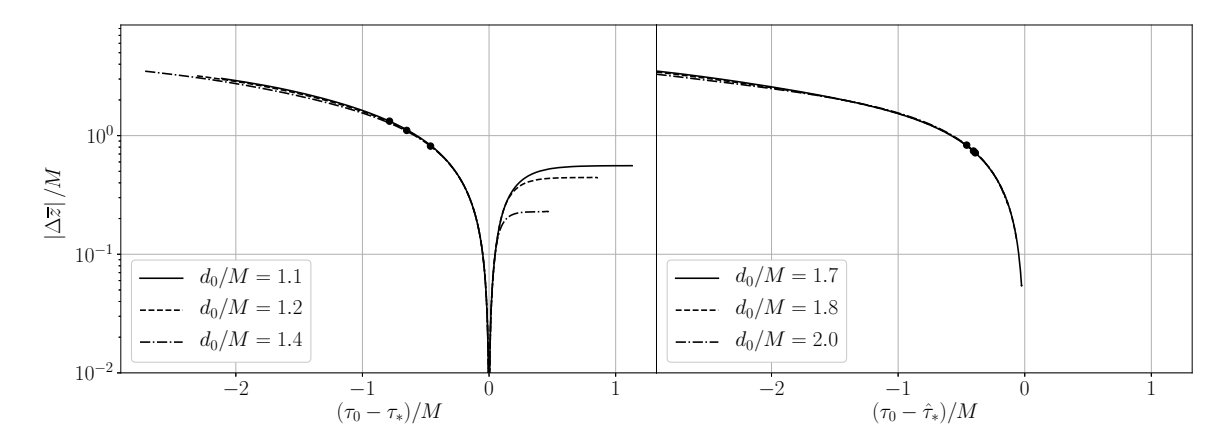
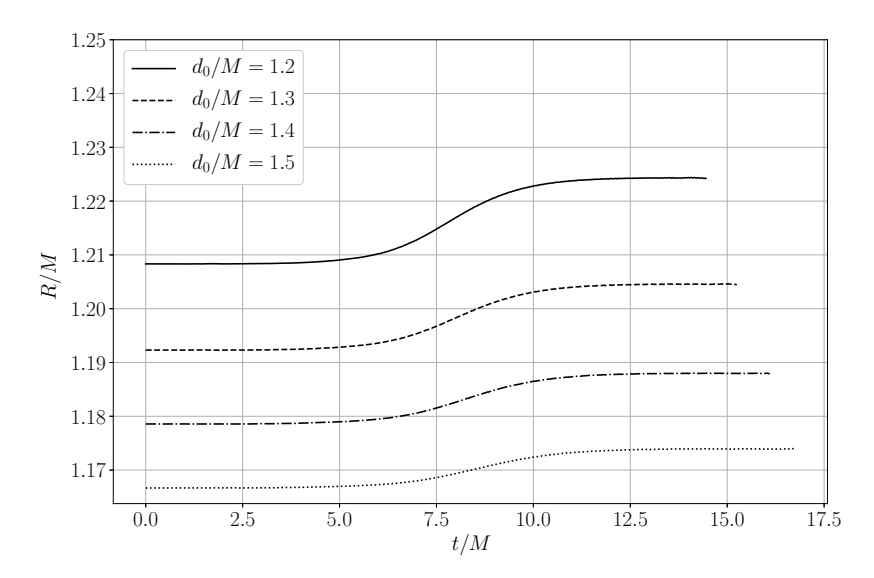


Figure 5. Proper separation  $|\Delta \bar{z}|$  between  $S_1$  and  $S_2$  for a few q=1 examples as a function of proper time  $\tau_0$  measured at the origin of the coordinate system. The left panel depicts three intersecting cases aligned at the time of intersection. The right panel shows three non-intersecting cases. Solid dots denote the time at which the common AH appears.

The insert shows extrapolation of  $\hat{\tau}_*/M$  beyond the intersecting cases, with three data points (solid dots) denoting non-intersecting cases in which  $\tau_f = \tau_0(t_f)$ , with  $t_f$  the time at the end of the simulation. Notice that  $\tau_f < \hat{\tau}_*$ , suggesting that, if in those cases the evolution had lasted  $\hat{\tau}_* - \tau_f$  longer, the surfaces would have intersected. The right panel in Fig. 4 shows  $\hat{\tau}_* - \tau_0$  as a function of coordinate time t for the three non-intersecting cases. Notice that  $\hat{\tau}_* - \tau_0 \to \text{constant}$ , as the lapse collapses, signaling that the progression of proper time has halted.

As mentioned before, tracking the separation or overlap of  $S_1$  and  $S_2$  with coordinate distances has the complication that the choice of gauge influences the outcome. To circumvent this, we show in Figure 5 the proper distance separation  $|\Delta \bar{z}|$  as a function of proper time  $\tau_0$  corresponding to the cases in Fig. 2. The left panel depicts the intersecting cases with time shifted by the time at intersection,  $\tau_*$ . The right panel shows three non-intersecting cases with the time also shifted but in this case by  $\hat{\tau}_*$  from the fit in Fig. 4. It is clear from both panels that for  $\tau_0 - \tau_* < 0$  and  $\tau_0 - \hat{\tau}_* < 0$ , the proper separation is independent of  $d_0$ . Also, if we were to combine the data from both panels, it would show that for these times all cases lie on top of each other; thus, there is no difference between intersecting and non-intersecting cases. Therefore, here again the data suggest that, if the evolutions for the non-intersecting cases had proceeded, the surfaces would have eventually intersected. The differences in  $|\Delta \bar{z}|$  with  $d_0$  arise when  $\tau_0 - \tau_* > 0$ , namely when the surfaces overlap. The left panel shows that at late times  $\mathcal{S}_1$  and  $\mathcal{S}_2$  reach a constant proper overlap, the smaller the value of  $d_0$  the larger the overlap. Furthermore, we find that the final overlap volume is never large enough to contain the punctures; they remain in the non-overlapping regions.

To gain further insight about the final state of the MOTSs and punctures, we show in Fig. 6 the evolution of the areal radius  $R = \sqrt{A/4\pi}$  with A the area of the MOTS for



**Figure 6.** Evolution of the areal radius of  $S_1$  for intersecting cases with q = 1. The areal radius of  $S_2$  is the same as that for  $S_1$  since the holes have equal masses.

a few intersecting cases with q = 1. It is clear that toward the end of the simulation, the surfaces  $S_1$  and  $S_2$  reach a constant areal radius and thus become isolated horizons [1]. This together with the finding that  $S_1$  and  $S_2$  have a constant proper overlap strongly suggest that the configuration is essentially frozen and the punctures will not merge.

## 5. Conclusions

We have presented results from a two-parameter study (mass ratio q and initial separation  $d_0$ ) of head-on collisions of BHs. The focus was on the ultimate fate of the MOTSs  $S_1$  and  $S_2$  that initially were the AHs of the colliding BHs. Depending on the values of q and  $d_0$ , once inside the common AH the surfaces  $\mathcal{S}_1$  and  $\mathcal{S}_2$  intersect if the lapse function  $\alpha_0$  takes longer to collapse before the end of the simulation. The collapse of the lapse is intrinsic to the singularity avoidance properties of the moving puncture gauge condition [16, 17] used in the simulations. We find that at late times for all cases, the coordinate separation of the BH punctures and of the MOTS surfaces  $S_1$ and  $S_2$  decrease  $\propto e^{-t/\lambda}$  with  $\lambda \approx 2M$ . When the separation of  $S_1$  and  $S_2$  is measured by proper distances, we find that at early times all cases exhibit the same behavior as a function of proper time. The data suggest that, if it were not for the collapse of the lapse, all cases would intersect. Furthermore, at late times the intersection or overlap freezes. Similarly, at late times, the areal radius of  $S_1$  and  $S_2$  reach a constant, thus becoming isolated horizons. These two facts, the freezing of the areal radius and the overlap, strongly suggest that the punctures do not merge. However, since this occurs at very small separations,  $(|\Delta z| \sim 10^{-4} M)$ , for practical purposes, the two punctures act as a single puncture, namely the singularity of the final BH.

## Acknowledgments

We would like to thank Abhay Ashtekar for useful discussions. This work was supported by NSF grants 1806580, 1550461, and XSEDE allocation TG-PHY120016.

#### References

- [1] Abhay Ashtekar and Badri Krishnan. Isolated and Dynamical Horizons and Their Applications. Living Reviews in Relativity, 7(1):10, December 2004.
- [2] Olaf Dreyer, Badri Krishnan, Deirdre Shoemaker, and Erik Schnetter. Introduction to isolated horizons in numerical relativity. *Physical Review D*, 67(2):024018, January 2003.
- [3] Abhay Ashtekar, Jonathan Engle, Tomasz Pawlowski, and Chris Van Den Broeck. Multipole moments of isolated horizons. *Classical and Quantum Gravity*, 21(11):2549–2570, April 2004.
- [4] Abhay Ashtekar, Miguel Campiglia, and Samir Shah. Dynamical black holes: Approach to the final state. *Physical Review D*, 88(6):064045, September 2013.
- [5] Anshu Gupta, Badri Krishnan, Alex B. Nielsen, and Erik Schnetter. Dynamics of marginally trapped surfaces in a binary black hole merger: Growth and approach to equilibrium. *Physical Review D*, 97(8):084028, April 2018.
- [6] José Luis Jaramillo, Rodrigo P. Macedo, Philipp Moesta, and Luciano Rezzolla. Black-hole horizons as probes of black-hole dynamics. II. Geometrical insights. *Physical Review D*, 85(8):084031, April 2012.
- [7] José Luis Jaramillo, Rodrigo P. Macedo, Philipp Moesta, and Luciano Rezzolla. Black-hole horizons as probes of black-hole dynamics. I. Post-merger recoil in head-on collisions. *Physical Review D*, 85(8):084030, April 2012.
- [8] J. L. Jaramillo, R. P. Macedo, P. Moesta, and L. Rezzolla. Towards a cross-correlation approach to strong-field dynamics in black hole spacetimes. AIP Conference Proceedings, 1458(1):158–173, July 2012.
- [9] Vaishak Prasad, Anshu Gupta, Sukanta Bose, Badri Krishnan, and Erik Schnetter. News from horizons in binary black hole mergers. arXiv e-prints, page arXiv:2003.06215, March 2020.
- [10] Abhay Ashtekar and Badri Krishnan. Dynamical horizons and their properties. *Physical Review* D, 68(10):104030, November 2003.
- [11] Erik Schnetter, Badri Krishnan, and Florian Beyer. Introduction to dynamical horizons in numerical relativity. *Physical Review D*, 74(2):024028, July 2006.
- [12] José Luis Jaramillo, Marcus Ansorg, and Nicolas Vasset. Application of initial data sequences to the study of Black Hole dynamical trapping horizons. AIP Conference Proceedings, 1122(1):308– 311. May 2009.
- [13] P. Mösta, L. Andersson, J. Metzger, B. Szilágyi, and J. Winicour. The merger of small and large black holes. *Classical and Quantum Gravity*, 32(23):235003, 2015.
- [14] Daniel Pook-Kolb, Ofek Birnholtz, Badri Krishnan, and Erik Schnetter. Existence and stability of marginally trapped surfaces in black-hole spacetimes. *Physical Review D*, 99(6):064005, March 2019.
- [15] Steven Brandt and Bernd Brügmann. A simple construction of initial data for multiple black holes. *Phys. Rev. Lett.*, 78:3606–3609, May 1997.
- [16] M. Campanelli, C. O. Lousto, P. Marronetti, and Y. Zlochower. Accurate Evolutions of Orbiting Black-Hole Binaries without Excision. *Physical Review Letters*, 96(11):111101, March 2006.
- [17] John G. Baker, Joan Centrella, Dae-Il Choi, Michael Koppitz, and James van Meter. Gravitational-Wave Extraction from an Inspiraling Configuration of Merging Black Holes. *Physical Review Letters*, 96(11):111102, March 2006.
- [18] Abhay Ashtekar and Gregory J. Galloway. Some uniqueness results for dynamical horizons.

  Advances in Theoretical and Mathematical Physics, 9(1):1–30, January 2005.

[19] Abhay Ashtekar, Christopher Beetle, and Stephen Fairhurst. Mechanics of isolated horizons. Classical and Quantum Gravity, 17(2):253–298, December 1999.

- [20] Jeffrey M. Bowen and James W. York. Time-asymmetric initial data for black holes and black-hole collisions. *Physical Review D*, 21(8):2047–2056, April 1980.
- [21] Daniel Pook-Kolb, Ofek Birnholtz, Badri Krishnan, and Erik Schnetter. Interior of a Binary Black Hole Merger. *Physical Review Letters*, 123(17):171102, October 2019.
- [22] Daniel Pook-Kolb. Self-intersecting marginally outer trapped surfaces. *Physical Review D*, 100(8), 2019.
- [23] Dieter R. Brill and Richard W. Lindquist. Interaction Energy in Geometrostatics. *Physical Review*, 131(1):471–476, July 1963.
- [24] Richard W. Lindquist. Initial-Value Problem on Einstein-Rosen Manifolds. *Journal of Mathematical Physics*, 4(7):938–950, July 1963.
- [25] Tom Goodale, Gabrielle Allen, Gerd Lanfermann, Joan Masso, Thomas Radke, Edward Seidel, and John Shalf. The Cactus Framework and Toolkit: Design and Applications. In *VECPAVector* and Parallel Processing R'2002, 5th International Conference, Berlin, 2003. Springer.
- [26] Sascha Husa, Ian Hinder, and Christiane Lechner. Kranc: A Mathematica package to generate numerical codes for tensorial evolution equations. *Computer Physics Communications*, 174(12):983–1004, June 2006.
- [27] Roland Haas, Roman V. Shcherbakov, Tanja Bode, and Pablo Laguna. Tidal Disruptions of White Dwarfs from Ultra-close Encounters with Intermediate-mass Spinning Black Holes. *The Astrophysical Journal*, 749(2):117, 2012.
- [28] Christopher Evans, Pablo Laguna, and Michael Eracleous. Ultra-close Encounters of Stars with Massive Black Holes: Tidal Disruption Events with Prompt Hyperaccretion. *The Astrophysical Journal Letters*, 805(2):L19, 2015.
- [29] Michael Clark and Pablo Laguna. Bowen-York-type initial data for binaries with neutron stars. *Physical Review D*, 94(6):064058, September 2016.
- [30] Karan Jani, James Healy, James A. Clark, Lionel London, Pablo Laguna, and Deirdre Shoemaker. Georgia tech catalog of gravitational waveforms. Classical and Quantum Gravity, 33(20):204001, 2016.
- [31] Thomas W. Baumgarte and Stuart L. Shapiro. Numerical integration of Einstein's field equations. *Physical Review D*, 59(2):024007, December 1998.
- [32] Erik Schnetter, Scott H. Hawley, and Ian Hawke. Evolutions in 3D numerical relativity using fixed mesh refinement. Classical and Quantum Gravity, 21(6):1465, 2004.
- [33] Erik Schnetter, Peter Diener, Ernst Nils Dorband, and Manuel Tiglio. A multi-block infrastructure for three-dimensional time-dependent numerical relativity. *Classical and Quantum Gravity*, 23(16):S553, 2006.
- [34] Maria Babiuc-Hamilton, Steven R. Brandt, Peter Diener, Matthew Elley, Zachariah Etienne, Giuseppe Ficarra, Roland Haas, Helvi Witek, Miguel Alcubierre, Daniela Alic, Gabrielle Allen, Marcus Ansorg, Luca Baiotti, Werner Benger, Eloisa Bentivegna, Sebastiano Bernuzzi, Tanja Bode, Bernd Bruegmann, Giovanni Corvino, Roberto De Pietri, Harry Dimmelmeier, Rion Dooley, Nils Dorband, Yaakoub El Khamra, Joshua Faber, Toni Font, Joachim Frieben, Bruno Giacomazzo, Tom Goodale, Carsten Gundlach, Ian Hawke, Scott Hawley, Ian Hinder, Sascha Husa, Sai Iyer, Thorsten Kellermann, Andrew Knapp, Michael Koppitz, Gerd Lanferman, Frank Lffler, Joan Masso, Lars Menger, Andre Merzky, Mark Miller, Philipp Moesta, Pedro Montero, Bruno Mundim, Andrea Nerozzi, Christian Ott, Ravi Paruchuri, Denis Pollney, David Radice, Thomas Radke, Christian Reisswig, Luciano Rezzolla, David Rideout, Matei Ripeanu, Erik Schnetter, Bernard Schutz, Ed Seidel, Eric Seidel, John Shalf, Ulrich Sperhake, Nikolaos Stergioulas, Wai-Mo Suen, Bela Szilagyi, Ryoji Takahashi, Michael Thomas, Jonathan Thornburg, Malcolm Tobias, Aaryn Tonita, Paul Walker, Mew-Bing Wan, Barry Wardell, Miguel Zilho, Burkhard Zink, and Yosef Zlochower. The einstein toolkit, October 2019. To find out more, visit http://einsteintoolkit.org.

[35] Jonathan Thornburg. A fast apparent horizon finder for three-dimensional Cartesian grids in numerical relativity. Classical and Quantum Gravity, 21(2):743, 2004.

- [36] Mark Hannam, Sascha Husa, Denis Pollney, Bernd Brügmann, and Niall Ó Murchadha. Geometry and Regularity of Moving Punctures. *Physical Review Letters*, 99(24):241102, December 2007.
- [37] Bernd Brügmann. Schwarzschild black hole as moving puncture in isotropic coordinates. *General Relativity and Gravitation*, 41(9):2131–2151, September 2009.
- [38] Mark Hannam, Sascha Husa, Frank Ohme, Bernd Brügmann, and Niall Ó Murchadha. Wormholes and trumpets: Schwarzschild spacetime for the moving-puncture generation. *Physical Review D*, 78(6):064020, September 2008.